Experimental investigation of Fe-clay/organic interactions under asteroidal conditions

J.-C. Viennet, Corentin Le Guillou, L. Remusat, F. Baron, L. Delbes, Anne-Marie Blanchenet, B. Laurent, I. Criouet, S. Bernard

Experimental investigation of Fe-clay/organic interactions under asteroidal conditions

J.-C. Viennet[1], C. Le Guillou[2], L. Remusat[1], F. Baron[3], L. Delbes[1], A.M. Blanchenet[2], B. Laurent[1], I. Criouet[1], S. Bernard[1]

[1] Muséum National d'Histoire Naturelle, Sorbonne Université, UMR CNRS 7590, Institut de minéralogie, de physique des matériaux et de cosmochimie, Paris, France.

[2] Univ. Lille, CNRS, INRA, ENSCL, UMR 8207 - UMET - Unité Matériaux et Transformations, F-59000 Lille, France.

[3] Institut de Chimie des Milieux et Matériaux de Poitiers (IC2MP), UMR 7285 CNRS, Université de Poitiers, F-86073 Poitiers Cedex 9, France.

∗ Corresponding author at: Muséum National d'Histoire Naturelle, Sorbonne Université, CNRS, UMR 7590, Institut de Minéralogie, Physique des Matériaux et Cosmochimie, Paris, France.

E-mail address: jean.christophe.viennet25@gmail.com (J.-C. Viennet).

Keywords

Clay minerals, Organic-mineral interaction; Hydrothermal alteration, Asteroids, Carbonaceous chondrites.

Abstract

Carbonaceous chondrites contain both soluble and insoluble organic materials (SOM and IOM) which may have been produced in different environments via different processes or share possible genetic relationships. The SOM may have been produced from IOM during hydrothermal episodes on asteroids, and *vice versa.* The potential role played by the mineral matrix during these episodes (clay minerals of variable crystallinity) remains to be constrained. Here, we exposed a mixture of formaldehyde and glycolaldehyde with ammonia-bearing liquid water together with Fe-rich smectitic minerals to hydrothermal conditions mimicking asteroidal conditions. We used both amorphous gel of smectite or crystalline smectites in order to understand the influence of the crystallinity on the evolution of OM. The organo-mineral experimental residues were characterized at a multiple length scales using X-ray diffraction and microscopy/spectroscopic tools. Results evidence that some IOM polymerizes/condenses in the absence of Fe-rich smectites. Yet, the presence of Fe-rich smectites inhibits this production of IOM. Indeed, the interactions between the SOM and clay surfaces (interlayers or edges) reduce the concentration of SOM available for polymerization/condensation reactions, a necessary step for the production of IOM. In addition, the presence of OM disorganizes the crystallization of the Fe-rich amorphous silicates, leading to smaller crystal sized particles exhibiting a lower permanent charge. This might suggests that the smectite permanent charge distribution may help better constraining the origin and evolution of chondritic clay minerals. Altogether, the present study sheds new light on the organo-mineral interactions having occurred during hydrothermal episodes onto/within chondritic asteroids. Indeed, IOM formation from OM-rich aqueous fluids does not occur during the alteration of amorphous silicates. This would mean that IOM is either produced within pockets free of clay minerals or initially accreted as IOM-rich grain. Last, about ~50 wt.% of the initial C could not be removed from the clay minerals at the end of the experiments using classical solvent extraction protocols, demonstrating that a high fraction of the SOM in carbonaceous chondrites may have been overlooked.

1. Introduction

Carbonaceous chondrites (CC) contain up to 5 wt. % of organic matter (OM) dominated by an insoluble fraction (IOM - 75 to 90 wt. %) associated with a minor soluble fraction (SOM - 10 to 25 wt%) (Robert and Epstein, 1982; Pearson et al., 2006; Alexander et al., 2007, 2017; Sephton, 2014; Remusat, 2015). While the SOM is composed of a diversity of small organic molecules (such as carboxylic acids, amino acids, nucleobases, polycyclic aromatic hydrocarbons, sugars…) (Pizzarello et al., 2006), the IOM consists in high molecular weight molecules made of aromatic units and short aliphatic chains rich in hetero-elements (Cody and Alexander, 2005; Remusat et al., 2005a; Remusat et al., 2019; Alexander et al., 2007; Derenne and Robert, 2010; Vinogradoff et al., 2017).

The possible genetic relationships between the SOM and the IOM remains a subject of investigations, notably because these compounds, potentially produced in different environments via different processes (Kerridge, 1993; Remusat et al., 2009; Aléon, 2010), have undergone multiple processes since their accretion onto/by parent bodies (McSween, 1979; Brearley, 2006; Danger et al., 2021). In fact, the presence of mineral products of hydrothermal alteration (e.g., smectite and/or serpentine phyllosilicates, carbonates and/or sulfides) have been reported in all CCs (Brearley, 2006; Le Guillou and Brearley, 2014; Le Guillou et al., 2014; King et al., 2015; Yesiltas and Kebukawa, 2016; Vinogradoff et al., 2017; Changela et al., 2018; Dionnet et al., 2018; Nittler et al., 2019; Vollmer et al., 2020).

Recent laboratory experiments demonstrated that IOM may form from SOM under asteroidal hydrothermal conditions. In fact, when exposed to 150°C, a mixture of formaldehyde and glycolaldehyde within liquid water containing ammonia will evolve into a diversity of soluble

compounds together with macromolecular organic solids sharing similarities with the chondritic IOM through formose and condensation reactions (Cody et al., 2011; Kebukawa et al., 2013, 2017, 2020; Kebukawa and Cody, 2015). Similar results were obtained using HMT (Hexamethylenetetramine - Vinogradoff et al., (2018)), i.e. the main product component of interstellar ice analogs (Bernstein et al., 1995; Cottin et al., 2001; Vinogradoff et al., 2011). This molecule decomposes into formaldehyde and ammonia in water at temperature > 70 °C (Meissner et al., 1954; Blazzevjic et al., 1979) producing solid macromolecular carbon insoluble in organic solvents within a few days at 150°C (Vinogradoff et al., 2018).

Yet, the possible role played by smectites in the production of IOM from SOM under asteroidal hydrothermal conditions (i.e. ~50 to ~200°C - Brearley, (2006)) requires further investigations. In fact, smectites closely associated to OM have been reported in chondrite matrices (Pearson et al., 2006; Garvie and Buseck, 2007; Le Guillou and Brearley, 2014; Le Guillou et al., 2015; Yesiltas and Kebukawa, 2016; Vinogradoff et al., 2017; Changela et al., 2018) and recent experimental studies have revealed that smectitic clay minerals may have a strong influence on organic reactions under hydrothermal conditions (Viennet et al., 2019, 2020; Vinogradoff et al., 2020a, b). While OM may influence smectite crystallization (Jacquemot et al., 2019), clay minerals may promote/catalyze various organic reactions (including cyclization, dehydration, Michael-addition…) even at temperatures below 100°C (Nagendrappa, 2011; Nagendrappa and Chowreddy, 2021). This is particularly the case of Fe-rich clay minerals, because the reactivity of some organic reactions in liquid water are enhanced in appropriate redox conditions (Lewan, 1997; Seewald, 2001; Mccollom and Seewald, 2006; Pan et al., 2009; McCollom et al., 2010; Lewan and Roy, 2011; Foustoukos and Stern, 2012; McCollom, 2013).

Here, we document the hydrothermal evolution of a mixture of formaldehyde and glycolaldehyde

within liquid water containing ammonia in the presence of Fe-rich smectitic phase, either amorphous or crystalline. The organo-mineral experimental residues were characterized at a multiple length scale using X-ray diffraction and advanced microscopy and spectroscopy tools, including infrared spectroscopic, scanning electron microscopy, scanning transmission X-ray microscopy coupled with X-ray absorption near edge spectroscopy and scanning transmission electron microscopy coupled with energy dispersive X-ray spectroscopy.

2. Materials and methods

2.1. Starting Materials

The organic starting material used for the present experiments is similar to that of previous studies (Cody et al., 2011; Kebukawa et al., 2013, 2017, 2020; Kebukawa and Cody, 2015). As done by Ricardo (2004), paraformaldehyde (1.5 mmol - 45 mg - Sigma Aldrich) and glycolaldehyde (1.5 mmol - 45 mg - Sigma Aldrich) were mixed within 2mL of pure water in which was added 12 mg of $Ca(OH)_2$ (Sigma Aldrich). Nitrogen was added as NH_4OH (20 µl - 14.8N - Sigma Aldrich) establishing the initial atomic N/C value at 0.1 (33 wt.% of C and 3.8 wt.% of N).

Pure nontronite ($Na_{0.4}(Fe(III)_2)(Si_{3.6}Fe(III)_{0.4})O_{10}(OH)_2$) was used as the Fe-rich smectitic mineral phase. An amorphous gel of nontronite was obtained by mixing $SiNa_2O_3.5H_2O$ (Sigma Aldrich) and $Fe(III)Cl_3.6H_2O$ (Sigma Aldrich) following the procedure detailed in Baron et al. (2016) and Petit et al. (2017). Salts and cations in excess were removed via filtration. The crystalline nontronite was synthesized by submitting the amorphous gel of nontronite to hydrothermal conditions (3 days at 150°C - Water/Gel of 3/50) in PTFE Parr© reactors. Washing with dichloromethane was performed to remove potential organic contamination. These mineral starting materials were then dried at room temperature (~ 25°C) over a day.

2.2. Laboratory Experiments

A first experiment was conducted in the absence of mineral. Confirming previous studies (Kebukawa and Cody, 2015), this experiment led to the production of IOM. For the experiments with minerals, 100 mg of either the crystalline nontronite or the nontronite gel were added to the 2 mL solution containing the organic mixture. These organo-mineral mixtures were introduced within titanium Parr© reactors loaded with 1 bar of Ar before closure and placed at 150 °C for 3 days (making them reach an authigenic water pressure of 5 bars). Note that, the NH_4OH solution was introduced the latest, just before closing the reactors to avoid degassing of NH_3(g). In agreement with previous studies (Baron et al., 2016), after 3 days at 150 °C, the amorphous gel crystallizes in the absence of the organic mixture (Baron et al., 2016) and the IOM yield is maximal in the absence of mineral (Kebukawa and Cody, 2015).

The experimental residues were filtered and washed with ultrapure water and dichloromethane (DCM) to remove the free soluble organic compounds (i.e. the soluble organic compounds not retained by the solid phases) and dried under vacuum (3.10^{-4} mBar) before characterization. Ten milligrams of each solid residue were subjected to HF/HCl dissolution protocols (Remusat et al., 2005b) to isolate the IOM possibly produced during the experiments. A 2:1 volume ratio HF/HCl (16/2 N) treatment was conducted for 24 hours, at room temperature. Note that, no IOM was recovered from the experiments with minerals. Control experiments without the organic mixture were also conducted to ensure the absence of contamination (Table S1 - Figure S1).

2.3. Characterization techniques

136 *2.3.1. Elemental analyses*

137 Total carbon and nitrogen contents were determined using a Flash2000, Thermo Fisher, elemental
138 analyzer operating at the Service de Spectrometry de Masse Isotopique du Museum (SSMIM) at
139 MNHN in Paris (France). A mass of 1 mg of each residue was combusted under oxygen/helium
140 flux at 1020°C. The N_2 and CO_2 released by combustion were separated by a chromatography
141 column and quantified using a thermal conductivity detector. Alanine was used as standard giving
142 uncertainties at 0.1 wt. % for N and 0.2 wt. % for C.

143 *2.3.2. XRD*

144 The X-ray diffraction (XRD) patterns were obtained on a Panalytical X'pert Pro MPD 2 circles
145 operating at IMPMC (Paris, France) The divergence slit, the anti-scatter slit and the two Soller slits
146 were set at 0.5°, 1°, 0.04° and 0.04 radian, respectively. The bulk XRD measurements were
147 performed on powder preparations throughout the 3-65 °2θ CoK$\alpha_{1,2}$ angular range (step size of
148 0.033 °2θ, counting time per step of 250 ms). The experiments dedicated to OM location were
149 performed on oriented preparations at both atmospheric pressure and under vacuum (3.10^{-4}
150 atmosphere) at 20 °C using an Anton Parr HTK 1200 oven coupled to an EDWARDS RV3 pump
151 throughout the 3-12 °2θ CoK$\alpha_{1,2}$ angular range (step size of 0.033 °2θ, counting time per step of
152 250 ms).

153 *2.3.3. MIR*

154 Mid-infrared (MIR) spectra were recorded in the 400-4000 cm^{-1} range with a 4 cm^{-1} resolution
155 using a Nicolet 6700 FTIR spectrometer (IMPMC, Paris) equipped with a KBr beamsplitter and a
156 DTGS-KBr detector, under ambient conditions by averaging 200 scans obtained in attenuated total
157 reflectance (ATR) geometry using a Specac Quest ATR device fitted with a diamond internal
158 reflection element. Transmission MIR spectra were obtained in the 400-4000 cm^{-1} range with a 4

159 cm^{-1} resolution using a Nicolet™ iS™ 50 FTIR spectrometer (IMPMC, Paris) equipped with a KBr
160 beamsplitter, an Ever-Glo source and a DTGS-KBr detector, by averaging 200 scans from KBr
161 pellets dried at 110°C obtained by mixing 1 mg of samples with 150 mg of KBr (Sigma Aldrich).

162 *2.3.4. SEM*

163 Scanning electron microscopy (SEM) investigations were performed on powders deposited on
164 carbon tape using the SEM-FEG ZEISS ULTRA 55 (IMPMC, Paris) equipped with a Bruker EDS
165 QUANTAX detector (Bruker Corporation, Houston, TX, USA). Images shown here (secondary
166 electrons) were collected using an acceleration voltage below 2 kV, thereby preventing irradiation
167 damages.

168 *2.3.5. Cryo-ultramicrotomy*

169 Cryo-ultramicrotome sections (100 nm thick) were prepared for X-ray absorption near edge
170 structure (XANES) and transmission electron microscopy (STEM) investigations using a Leica
171 cryo-ultramicrotome at UMET (Lille, France) following a recently developed protocol (Jacquemot
172 et al., 2019; Viennet et al., 2019, 2020). Powders of experimental residues were mixed with 0.1 ml
173 of deionized water, then a drop of the mixture was frozen in liquid nitrogen at -120 °C and cut. The
174 ultrathin slices of residues were then deposited on holey carbon film TEM grids (coated with a ~3
175 nm chromium layer).

176 *2.3.6. XANES*

177 XANES data were collected using the HERMES STXM beamline at the synchrotron SOLEIL
178 (Belkhou et al., 2015; Swaraj et al., 2017). Beamline optical elements were exposed to a continuous
179 flow of pure O_2 to remove carbon contamination. Energy calibration was done before
180 measurements using the well-resolved 3p Rydberg peak of gaseous CO_2 at 294.96 eV. XANES
181 data were extracted from image stacks collected at energy increments of 0.1 eV over the carbon

(270–350 eV) absorption range with a dwell time of ≤ 1 ms per pixel to prevent irradiation damage (Wang et al., 2009). Alignment of stack images and extraction of XANES spectra were done using the aXis2000 software. The C-XANES spectra shown here correspond to homogenous carbon-rich areas of several hundreds of square nanometers. Following the method described in Le Guillou et al. (2018), background was subtracted using a power law before spectra were normalized to the carbon quantity by integrating the spectra from the pre-edge region up to the mean ionization energy (e.g. 282.0-291.5 eV at the C K edge).

2.3.7. TEM

Scanning transmission electron microscopy (STEM) and electron dispersive spectroscopy (EDS) mapping were performed using a Thermofisher Titan Themis 300 microscope operated at 300 keV, at the "centre commun de microscopie – CCM" at the University of Lille. High resolution images were obtained in STEM mode using the high angle annular dark field detector (HAADF), a convergence angle of 20 mrad, a camera length of ~ 150 mm, a beam current below 200 pA and a dwell time between 5 and 10 µs. Hyperspectral EDS data were obtained using the super-X detector system equipped with four windowless silicon drift detectors. The probe current was set at 600 pA with a dwell time of 2 µs per pixel. A key aspect is the post-acquisition processing of the hyperspectral data, performed using the Hyperspy python-based package (de la Pena et al., 2017). The EDS spectrum at each pixel was fitted by a combination of Gaussian functions for the X-ray lines and a 6^{th} order polynomial function for the background. Quantification was achieved using the integrated intensities of the Gaussian through the Cliff-Lorimer method (Cliff and Lorimer, 1975), using experimentally determined k-factors. The thickness x density product strongly affects the X-ray reabsorption of the light elements (O, Fe_L). It was determined using the two-lines

204 method (Morris, 1980), which compares the quantification obtained from the Iron L-lines and Iron
205 K-lines and accurate absorption correction was performed.
206

3. Results

3.1. MIR spectra of the SOM

In the following, we focus on the characterization of the DCM-washed solid residues. Of note, only the residue produced in the absence of minerals contained IOM, although the free soluble organic compounds extracted using DCM exhibit very similar MIR spectra (Figure 1). The spectra exhibit stretching of O-H or N-H bonds at 3370 and 3200 cm^{-1}, of aliphatic C-H at 2959 cm^{-1} and 2920 cm^{-1}, of C-H of -O-CHx bonds at 2851 cm^{-1} (Kebukawa et al., 2020), N-H bonds in amide at 1567-1580 cm^{-1}, of C-H, C-N, O-H bonds at 1412, 1382, 1315 cm^{-1}, of C-O in alkoxy at 1043, 1076, 1120 cm^{-1}, and C-H bending in alkene at 928 and 770 cm^{-1}. Note that the MIR spectra of the initial OM exhibit important differences than for the free soluble organic compounds demonstrating the OM evolution due to the experimental hydrothermalism.

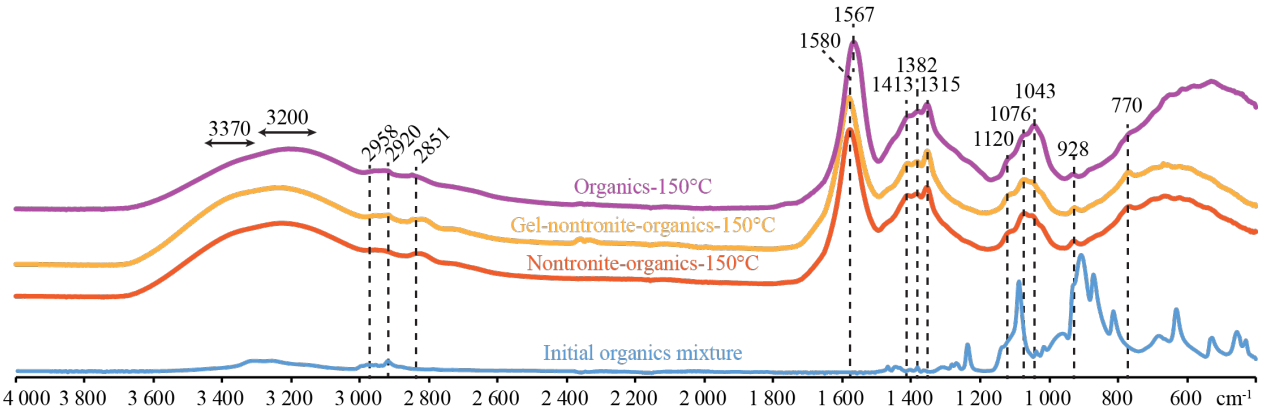

Figure 1: *ATR-MIR spectra of initial OM and of the free soluble organic compounds extracted using DCM from the experimental residues.*

223 **3.2. TOC and N/C**

224 Here, we focus on the characterization of the DCM-washed solid residues of experiments. The
225 experiments conducted in the absence of minerals lead to the production of a solid organic residue
226 insoluble in organic solvents, i.e. to the production of IOM. This IOM contains 65 wt.% of carbon
227 (24 % of the initial mass of carbon) and 7.3 wt.% of nitrogen (22.8 % of the initial mass of nitrogen).
228 In contrast, no IOM was recovered after the dissolution of the silicates using acid demineralization.
229 The solid residues produced in the presence of the crystalline nontronite or in the presence of the
230 gel of nontronite contain 14.3 and 14.1 wt.% of carbon (54.3 and 50.1 % of the initial carbon,
231 respectively) and 2 and 1.9 wt% of nitrogen (64.4 and 56.2 % of the initial nitrogen, respectively).
232 This OM exhibits slightly higher N/C values (0.12) than those of the starting organic material and
233 of the IOM produced in the absence of minerals (0.10).

Starting Materials	Organic-150°C	Nontronite Organics	Gel-nontronite Organics
Initial mass of organic mixture (mg)	102	102	102
Initial mass of minerals (mg)	0	100	100
Final mass of solids (mg)	12.4	127.7	119.8
Initial $\%_{wt}$ C	33.0	16.7	16.7
Final $\%_{wt}$ C	64.8	14.5	13.2
Initial mass of C (mg)	33.7	33.7	33.7
Final mass of C (mg)	8.0	18.5	15.8
Percentage of initial C trapped (%)	23.8	54.9	47.0
Initial $\%_{wt}$ N	3.8	1.9	1.9

Final % $_{wt}$ N	7.3	2.0	1.9
Initial mass of N (mg)	3.9	3.9	3.9
Final mass of N (mg)	0.9	2.5	2.2
Percentage of initial N trapped (%)	23.0	64.4	56.2
Final N/C of the solid residue	0.10	0.12	0.12
IOM	Yes	No	No

Table 1: Carbon and nitrogen contents in solid experimental residues and N/C values.

3.3. XRD

XRD provide information on the nature and crystallinity of the solid fraction of the residues (Figure 2). Nontronite is a smectite made of 2:1 layers composed of an octahedral sheet sandwiched between two tetrahedral sheets. Isomorphic substitution by a lower charge cation in the tetrahedral sheets (Si^{4+} substitution by Fe^{3+}) induces a negative charge, called "permanent charge". The latter is compensated by exchangeable cations present either within the interlayer space (originally Na^{+} here) or on the basal planes. In addition, other charges due to crystal defects, such as silanol bonds are present on the edges of the clay minerals sheets.

In the absence of the organic mixture, the gel of nontronite (initially amorphous, as indicated by its XRD pattern – Figure 2) crystallizes into a low charge nontronite, as attested by the XRD peaks at 4.55, 3.15, 2.59, 1.73 and 1.525 Å corresponding to the 0.2.11, 004, 13.20, 15.24.31 and 06.33 reflections of the crystalline nontronite (Baron et al., 2016). In contrast, in the presence of the organic mixture, the nontronite gel does not crystallize that well. The XRD pattern of the solid residue do not show the 001 reflection. The wide peaks at 4.37, 2.57 and 1.537 Å correspond to the 0.2.11, 13.20 and 06.33 reflections of a poorly crystalline nontronite (Baron et al., 2019). The

crystallinity of the crystalline nontronite also decreases during the experiments conducted in the presence of the organic mixture as evidenced by the broadening of the hkl reflections. In addition, the 001 reflection of the solid residue is shifted to 18.00 Å, likely due to mixed-layer stacking and/or trapping of OM into its interlayer space (Laird, 1994; Lagaly et al., 2013; Viennet et al., 2015, 2016, 2019, 2020; Gautier et al., 2017). Such trapping of organic carbon within the interlayer spaces of the nontronites seems to be confirmed by XRD measurements performed under vacuum (Figure 3). In fact, under vacuum, the distance corresponding to the 001 reflection of the residues produced in the presence of the organic mixture do not collapse, in contrast to that of the crystalline nontronite that were never exposed to the organic mixture. Indeed, only small shifts of their 001 reflections attest that the interlayer spaces of these smectites are locked by organic compounds (Viennet et al., 2019, 2020).

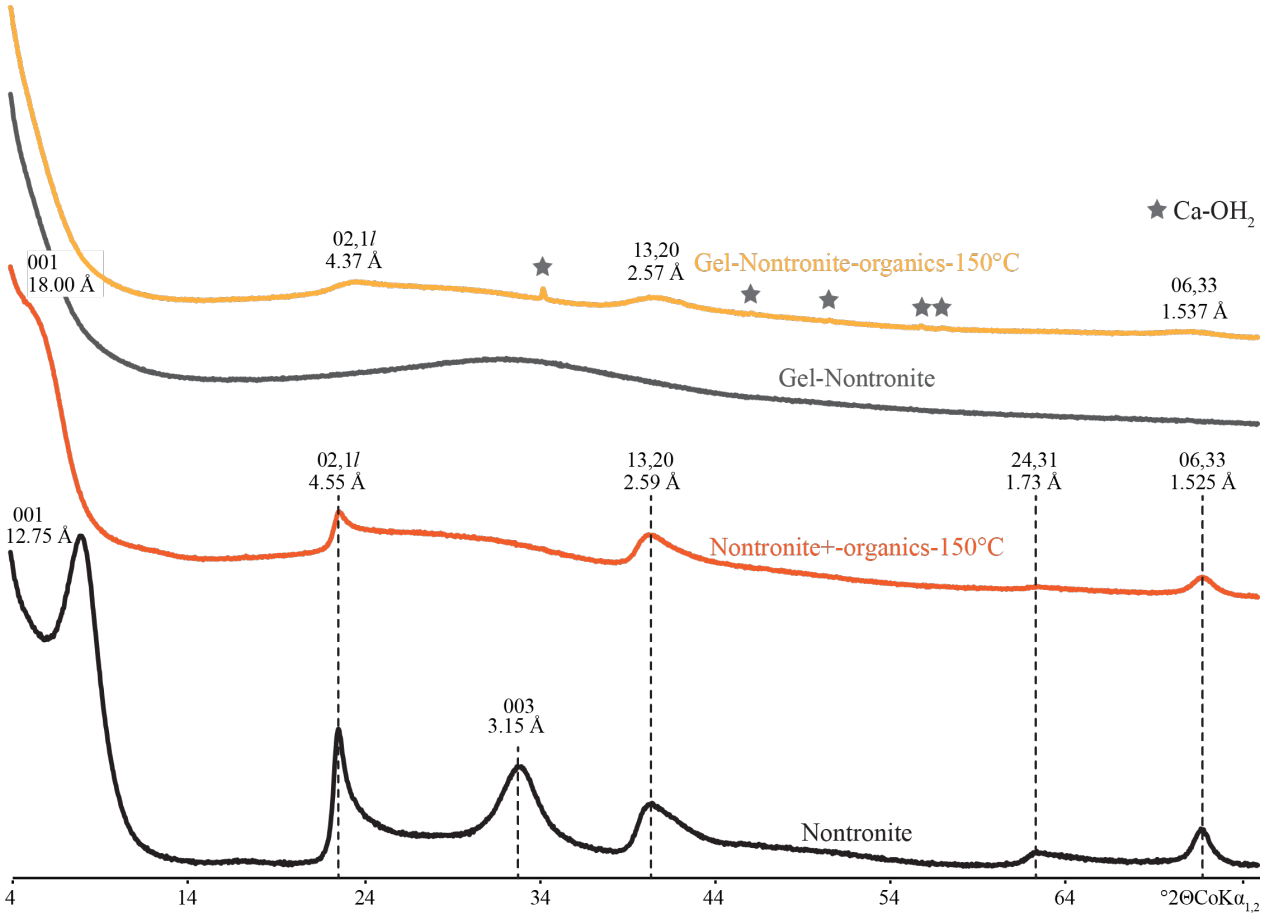

Figure 2: *XRD patterns of the starting gel of nontronite, the starting nontronite and the solid residues of experiments. The small peaks at 3.03, 2.49, 2.28, 2.09, 1.91, 1.87 Å (grey stars) are attributed to* $CaOH_2$.

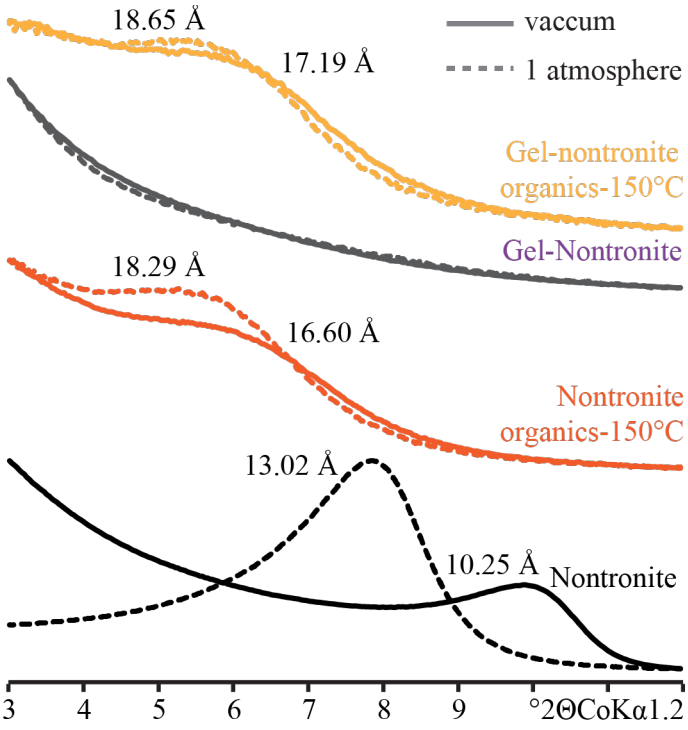

Figure 3: *XRD patterns under ambient pressure and under vacuum of the starting gel of nontronite, the starting nontronite, and the solid residues of experiments. Note that the 001 reflection of the residues produced in the presence of the organic mixture do not shift to ~10 Å under vacuum, indicating the presence of OM within the interlayer space of the nontronites.*

3.4. MIR

Transmission-MIR investigations in the 400-1300 cm^{-1} range confirm that, the crystalline nontronite is a low charge smectite (Figure 4). In fact, spectra show sharp bands attributed to stretching of Si-O (1008 cm^{-1}), bending of Fe^{3+}_2-OH (816 cm^{-1}), symmetrical stretching of Si-O-Si (780 cm^{-1}), $^{[4]}$Fe(III)-O vibrations (707 cm^{-1}), $^{[6]}$Fe(III)-O_{apical} vibrations (677cm^{-1}) and Si-O_{apical}-$^{[6]}$Fe(III) vibrations (around 600 cm^{-1}) (Farmer, 1974; Baron et al., 2016). Of note, below 600 cm^{-1} and at 840 cm^{-1}, the attribution of the vibration bands remains complex (Baron et al., 2016). The

band at 3630 cm^{-1} corresponds to the OH stretching vibrations of water molecules weakly bonded to the oxygen of the silicate lattice (Figure 4, Farmer and Russell, 1971). In addition, the bands at 1632, 3232 and 3353 cm^{-1}, correspond to the vibrations of OH bonds in H_2O. The MIR spectra of the solid residues produced in the presence of the organic mixture exhibit the main absorption bands of nontronite, but these bands are rather wide compared to the sharp bands of crystalline nontronite, also indicating a lower degree of crystallinity (Baron et al., 2016). Plus, the bands attributed to the stretching of Si-O bonds are shifted at 1028 and 1015 cm^{-1} for the residues produced with the crystalline nontronite and with the gel of nontronite, respectively, which can be explained by a slightly lower charge compared to that of the starting nontronite (Baron et al., 2016). A lower charge may also explain the lower intensity of the band at 677 cm^{-1} and the higher intensity of the band at 707 cm^{-1}, attributed to $^{[4]}$Fe(III)-O vibrations and $^{[6]}$Fe(III)-O_{apical} vibrations, respectively (Baron et al., 2016), while interactions with OM may explain the lower intensity of the band at 815 cm^{-1}, attributed to the bending of $Fe^{3+}{}_2$-OH bonds. Compared to those of crystalline nontronite, the spectra of the residues produced in the presence of the organic mixture exhibit a broader and less intense band at 3562 cm^{-1}, corresponding to the stretching of $Fe_2{}^{3+}$-OH in octahedral position (Baron et al., 2016). This evolution indicates either a lower degree of crystallinity and/or interactions of OM with the structural OH, which is consistent with transmission-MIR data. In addition, the band at 3630 cm^{-1}, corresponding to the stretching of OH vibrations of water molecules weakly bonded to the oxygen of the silicate lattice (Farmer and Russell, 1971), is weaker in presence of organics, indicating either a lower degree of crystallinity and/or interactions of OM with the edges of smectites.

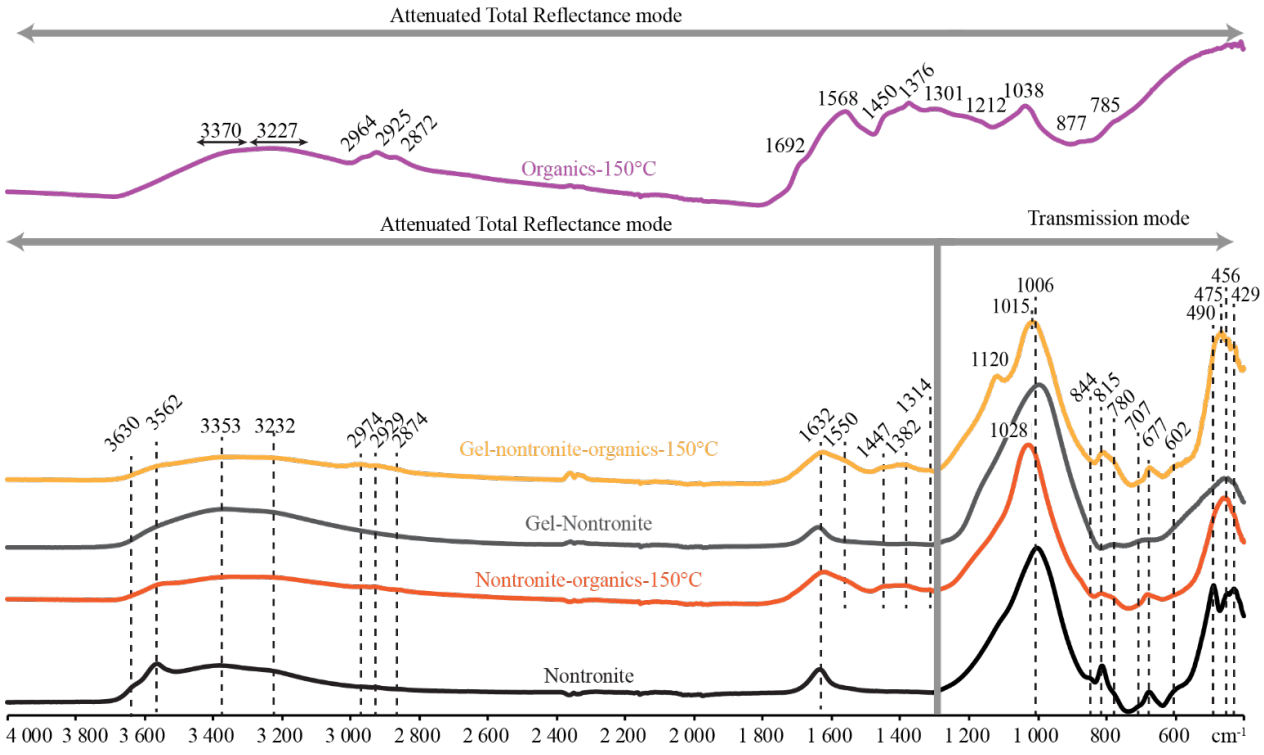

Figure 4: *Infrared spectra in ATR mode from 4000 to 1300 cm^{-1} and in transmission mode from 1300 to 400 cm^{-1} of the pristine materials, of the organo-minerals residues and the mineral-free experiment (organics-150°C, in purple).*

ATR-MIR spectra also provide information on the chemical nature of the organic fraction of the residues (Figure 4). In addition to a large band centered at 3227 cm^{-1} attributed to O-H bonds, the spectrum of the IOM produced in the absence of minerals shows bands at 1376 and 1450 cm^{-1} and at 2872, 2925 and 2964 cm^{-1} attributed to the bending and stretching of aliphatic C-H, bands at 785 and 877 cm^{-1} attributed to the bending of aromatic C-H, bands at 1038, 1212 and 1301 cm^{-1} attributed to the stretching of alcohol C-O, a band at 1692 cm^{-1} attributed to the stretching of amide/ester C=O and a band at 1556 cm^{-1} attributed to the bending of amide N-H (Bernard et al., 2015). In contrast, the spectra of the organic compounds trapped within the residues produced from

314 the organic mixture in the presence of the crystalline nontronite or the gel of nontronite show bands
315 at 1383 and 1447 cm^{-1} and at 2874, 2929 and 2974 cm^{-1} attributed to the bending and stretching of
316 aliphatic C-H (although the band at 1447 cm^{-1} may also be attributed to R-NH_3^+), a band at 1314
317 cm^{-1} attributed to the bending vibration of phenol C-O, and a band at 1550 cm^{-1} attributed to the
318 bending of amide N-H (Yariv and Cross, 2001; Gautier et al., 2017; Viennet et al., 2019, 2020).

319

320 **3.5. XANES**

321 The XANES spectra collected at the carbon edge on ultramicrotome sections also provide
322 information on the chemical nature of the organic fraction of the residues (Figure 5). The XANES
323 spectrum of the IOM produced in the absence of minerals shows peaks attributed to aromatic and
324 olefinic carbons (285.0 eV), conjugated aromatic cycles (285.5 eV), heterocycles (286.0 eV),
325 amine/imine/cyano groups and/or ketone and phenol groups (286.5 eV), aliphatic carbons (287.9
326 eV), amide groups (288.2 eV) and carboxylic groups (288.5 eV) (Alleon et al., 2017; Le Guillou
327 et al., 2018). No IOM was produced in the presence of the crystalline nontronite, the organic carbon
328 trapped within the solid residue exhibits different spectrum, with peaks at the same energies
329 indicating a roughly similar chemistry, although this carbon appears to contain a bit more aromatic
330 and/or olefinic carbons (285.1 eV), more phenol carbons (287.2 eV) and a bit more aliphatic
331 carbons (287.9-288.5 eV). The organic carbon trapped within the solid residue produced in the
332 presence of the gel of nontronite also contains more aromatic and/or olefinic carbons (285.0 eV)
333 and much more aliphatic carbons (287.9-288.5 eV) and amide groups (288.2), but less heterocycles
334 (285.9 eV) and less amine/imine/cyano groups and/or ketone and phenol groups (286.5 eV).

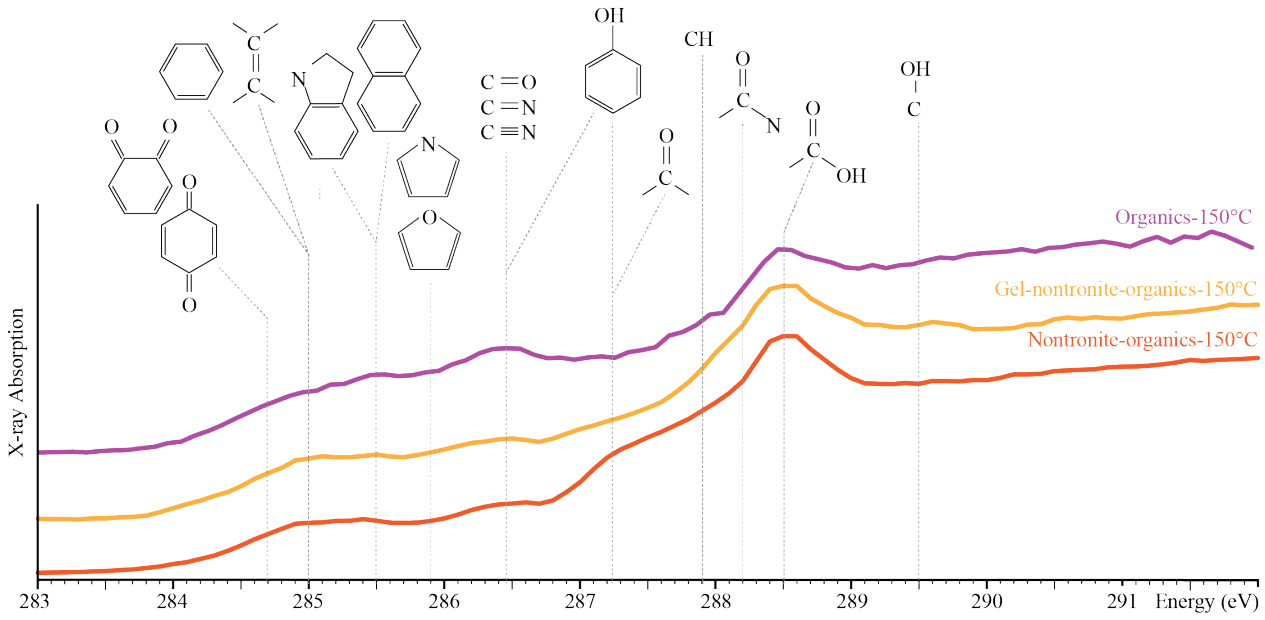

Figure 5: *XANES spectra of the solid experimental residues.*

3.5. SEM and TEM

SEM and TEM allowed comparing the textures and microstructures of the solid residues (Figure 6). At the micrometer scale, the solid residue produced in the presence of the crystalline nontronite displays the typical layered, flower-like texture of smectites while the solid residue produced in the presence of the gel of nontronite presents a rough and granular surface. These differences in texture correspond to differences in structure/crystallinity as revealed by TEM observations. At the TEM scale, while stacks of ~5 to ~10 layers (~ 10 nm thick along the 100 direction) extending laterally up to 100 nm can be observed within the solid residue produced in the presence of the crystalline nontronite, much smaller particles (< 10 nm) exhibiting less than 3-5 layers are observed within the solid residue produced in the presence of the gel of nontronite, in good agreement with XRD patterns and MIR data. Besides a few grains of $Ca(OH)_2$, both residues appear homogenous.

No individual organic carbon grain can be observed within the solid residues, but in addition to Fe, Si, O and Ca, STEM-EDS data show that carbon and nitrogen are intimately associated with minerals and homogeneously distributed within the solid residues. Although the starting crystalline nontronite contains Na compensating its permanent charge (Na/Si = 0.11), the solid residues do not contain any Na, the permanent charge of the smectites being likely compensated by nitrogen (originating from NH_4OH) and calcium (originating from $Ca(OH)_2$). The Fe/Si of the solid residues (0.58 and 0.62) are lower than that of the starting crystalline nontronite (0.66). Of note, considering the theoretical formula of nontronite ($M^+_x(Fe_2)(Si_{4-x}Fe_x)O_{10}(OH)_2$), the mean $^{[4]}$Fe/Si values correspond to permanent charges of 0.2 and 0.28 in the residue produced in the presence of the gel of nontronite and the crystalline nontronite, respectively. The charge of the starting crystalline nontronite was initially 0.4, confirming the interpretation of XRD and MIR results. Based on the study of (Dzene et al., 2017), even for synthetic samples with well-controlled chemistry, permanent

tetrahedral charge can be modeled by a distribution heterogeneity as highlighted in figure 6.f. The distribution of the permanent charge values appears a lot broader for the solid residue produced from crystalline nontronite compared to the thinner distribution for the solid residue produced from the nontronite gel.

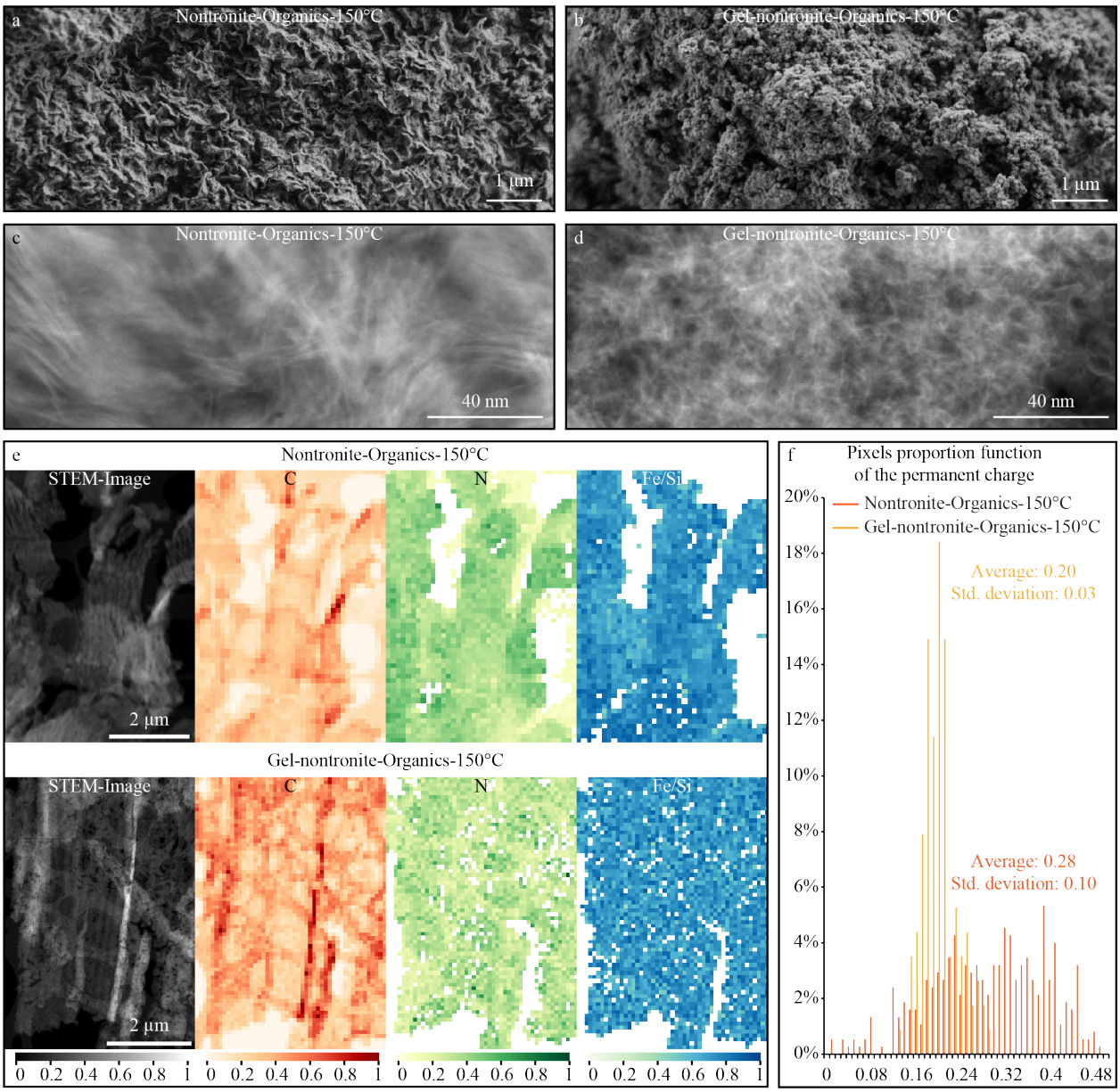

Figure 6: *(a-b) SEM and (c-d) STEM images of the organo-mineral residues. (e) Chemical maps of organo-mineral residues showing the association of carbon, nitrogen with the Fe-rich smectites and the more heterogeneous Fe/Si ratios of the Nontronite-organics-150°C residue compare to the the Gel-nontronite-organics-150°C residue. (f) Permanent charge distribution of the nontronite highlighting the more homogenous chemical composition of the Gel-nontronite-organics-150°C residue compare to the Nontronite-organics-150°C experiment.*

4. Discussion

4.1. Effect of organo-mineral interactions

In the absence of minerals, the organic mixture produces IOM when exposed to hydrothermal conditions at 150 °C for 3 days. This IOM accounts for ~ 10 % of the initial mass of the organic mixture (see Table 1). According to MIR and XANES data (Figures 4 & 5), this IOM contains aromatic cycles, heterocycles, amine/imine/cyano groups and/or ketone and phenol groups, aliphatic carbons, amide groups and carboxylic groups. The chemical structure of this IOM is thus similar to the organic solids produced in previous studies from the same starting material (Cody et al., 2011; Kebukawa et al., 2013; Kebukawa and Cody, 2015). Similarly to what occurred for HMT (Vinogradoff et al., 2018), the production of IOM from the organic mixture used here occurred via multiple reaction steps, including condensation, dehydration and cyclization reactions involving sugars produced from formaldehyde via the Formose reaction (Kort, 1970; Weber, 2001; Cody et al., 2011; Kebukawa et al., 2013; Kebukawa and Cody, 2015).

However, the present results show that the same mixture does not produce IOM when exposed to similar conditions in the presence of an amorphous gel of nontronite or in the presence of a crystalline nontronite. In fact, no organic solid is retrieved after the acid dissolution of the solid

391 residues investigated here. This is in agreement with results of a previous study, which indicated
392 that the soluble compounds produced from HMT exposed to hydrothermal conditions in the
393 presence of smectites have a lower molecular weight than those produced from HMT in the absence
394 of minerals (Vinogradoff et al., 2020). The DCM-washed solid residues investigated here contain
395 an important amount of C and N (Table 1), likely under the form of soluble compounds trapped
396 within the interlayer spaces of smectites (Figure 3) and/or adsorbed at the surface of smectites
397 (Figure 4). The organic compounds trapped within the residues are not drastically different from
398 the IOM produced in the absence of minerals from a chemical point of view. Nevertheless, the
399 organics trapped within the residues produced in the presence of the gel of nontronite are more
400 aliphatic and contain less phenol carbons (Figure 4 & 5).
401 The presence of organic compounds within the interlayer spaces of the smectites is attested by the
402 behavior of their 001 d-spacing under vacuum (Figure 3), while the presence of organic compounds
403 on the edges is attested by the lower absorption of the OH stretching vibrations of water molecules
404 weakly bonded to the oxygen of the silicate lattice (Figure 4). The quantity of organic compounds
405 trapped within the solid residues (about 50% of the initial C and more than 60% of the initial N) is
406 significant considering that only 10 % of the organic mixture is converted into IOM in the absence
407 of minerals (note that this is not a kinetic limitation - Kebukawa et al., 2013; Kebukawa and Cody,
408 2015). Such entrapment of nitrogen may have prevented formation of IOM as Kebukawa et al.
409 (2013) having noticed that high levels of nitrogen yield more IOM. In fact, because OM present in
410 the liquid phase and the organic compounds trapped within/onto clays minerals share similar
411 moieties (as revealed by MIR (Figures 1 and 4) and XANES data (Figure 5)), a threshold effect
412 could be proposed: if the concentration of the reactive species necessary to produce IOM through
413 polymerization/condensations reactions (Kebukawa et al., 2013) is not high enough, the reaction
414 may not proceed. Altogether, the present results demonstrate that the presence of smectitic

materials, independently of their degree of crystallinity, inhibits the production of IOM. This likely occurs by trapping organic compounds, hence limiting polymerization/condensation reactions. The presence of clay minerals has thus a strong influence on reactions between organic species.

The reciprocal is also true. When exposed to hydrothermal conditions at 150 °C for 3 days in the absence of the organic mixture, the crystalline nontronite remains crystalline while the gel of nontronite crystallizes (Figures 3 & 4). However, the presence of the organic mixture modifies these behaviors: the crystallinity of crystalline nontronite decreases during the experiments, while the gel of nontronite does not produce crystalline nontronite but rather small particles of low degree of crystallinity (Figures 3, 4 & 6). Similar behaviors were observed in experiments conducted with gels of (Al,Mg)-rich smectites in the presence of RNA (Jacquemot et al., 2019; Viennet et al., 2019, 2020). As is the case in these studies, the poorly crystalline smectites of the residues investigated here have retained organic compounds, both within their interlayer spaces (Figure 3 - Viennet et al., 2019, 2020) and at their surface (Figure 4 - Viennet et al., 2019, 2020). The smectites of the experimental residues exhibit lower Fe/Si values according to TEM data (Figure 6), indicating that their permanent charges (corresponding to the number of Si substitutions by $^{[4]}$Fe in the tetrahedral sheets) is lower than those of the starting crystalline nontronite. Such low permanent charge is also attested by the MIR results showing a shift of the band position of the Si-O bonds and the relative intensity decrease of the bands corresponding to the $^{[4]}$Fe-O bonds (Figure 4). The distinct distribution of the permanent charge values is also of interest. In contrast to the restricted distribution of the permanent charge values of the solid residue produced in the presence of the gel of nontronite, the solid residue produced in the presence of the crystalline nontronite exhibits a rather wide distribution of $^{[4]}$Fe/Si values, i.e. a highly variable permanent charge. By analogy with the production of lower charge clay minerals via the alteration of micas by organic acids (Jackson, 1962; Robert et al., 1979; Wilson, 1999), it can be assumed that this wide distribution reflects the

alteration by acid-complexation of Fe of the crystalline nontronite during the experiments. While, the sharper distribution of the solid residue produced in the presence of the gel of nontronite would reflect crystallization process from the gel as for smectites produced in inorganic media (Dzene et al., 2017). Of note, in contrast to crystallinity, the permanent charge of nontronites is pH dependent (Baron et al., 2016). The nontronite was synthesized at pH comprise between 12-11.5 (Baron et al., 2016). The presence of $CaOH_2$ in the starting materials of our experiments serves as a buffer for a pH at 11.5–11.7 (Kebukawa and Cody, 2015). Yet, such slight decrease of pH would not changes the permanent charge of the nontronites (Baron et al., 2016; Petit et al., 2017). This decrease is likely related to the presence of organic matter. In any case, the present results demonstrate that the presence of organic materials disturbs the crystallization of Fe-rich smectites possibly as observed with (Al,Mg)-rich smectites in the presence of RNA (Jacquemot et al., 2019) and/or via complexation as with iron oxides in soils (Schwertmann, 1966) and affects their permanent charge via the production of organic acids preventing/impacting tetrahedral substitutions (Baron et al., 2016).

4.2. Implications for carbonaceous chondrites

Asteroid parent bodies accreted organic molecules whose nature and diversity are not yet elucidated, notably because these bodies experienced a multitude of hydrothermal processes, having modified the initial nature of the accreted OM (Cody et al., 2011; Vollmer et al., 2014; Le Guillou and Brearley, 2014; Le Guillou et al., 2014; Vinogradoff et al., 2017). The possible genetic relationships between the SOM and the IOM thus remain a subject of speculations: it has been suggested for instance that soluble compounds have formed via the oxidation of solid (insoluble) organic compounds (Yabuta et al., 2007), that IOM have formed through the polymerization of soluble compounds (Kebukawa et al., 2013; Kebukawa and Cody, 2015; Kebukawa et al., 2020), and that phyllosilicates have played a key role in the chemical evolution of both soluble and

463 insoluble compounds (Le Guillou and Brearley, 2014; Le Guillou et al., 2014; Yesiltas and
464 Kebukawa, 2016; Changela et al., 2018; Vinogradoff et al., 2020a).
465 The present experimental results provide new clues for understanding the organo-mineral
466 interactions at work under hydrothermal conditions. In agreement with previous studies (Kebukawa
467 et al., 2013, 2017, 2020; Kebukawa and Cody, 2015), the production of IOM occurred during
468 experiments conducted with the organic mixture in the absence of minerals. Yet we show here that
469 the presence of clay minerals, either amorphous or crystalline, inhibits this production of IOM and
470 that the organic compounds trapped within the residues are more aliphatic than the IOM. This is
471 also the case of the diffuse OM intimately associated with clay minerals in chondrites, which has
472 been documented as more aliphatic than the IOM (Le Guillou and Brearley, 2014; Le Guillou et
473 al., 2014; Vinogradoff et al., 2017; Changela et al., 2018; Kebukawa et al., 2019; Dionnet et al.,
474 2020). The present results thus suggest that the chondritic IOM may have only form within pockets
475 from which clay minerals or amorphous precursors of clay minerals were absent and/or that IOM
476 grains may have pre-accretionary origins (Remusat et al., 2010).
477 The quantity of organic compounds trapped within the residues investigated here is significantly
478 higher than that of residues of experiments conducted by Vinogradoff et al. (2020) which produced
479 residues containing only 3-4 wt % of C. Although these experiments were conducted under similar
480 conditions, Vinogradoff et al. (2020) used HMT and Al or Fe-rich smectites. Altogether, those
481 results demonstrate the mutual effect of the crystallochemistry of smectites and the composition of
482 OM on the composition of the final organo-mineral assemblages. Plus, the present study evidences
483 that the initial crystallinity of the mineral phase also plays a role in the final chemistry and
484 quantities of the organic compounds eventually trapped within. The different trapping capacities
485 of different smectites may explain the highly heterogeneous nature of the matrices of carbonaceous
486 chondrites, both regarding the crystallochemistry of hydrated silicates and the quantity and

chemistry of diffuse OM trapped within these mineral phases (Le Guillou et al., 2014; Vinogradoff et al., 2017: Changela et al., 2018).

The presence of organics partially inhibits the growth of Fe-rich clay minerals such as nontronite (both the particle sizes and the degree of crystallinity of the smectitic clays are lower in residues produced in the presence of the organic mixture). Of note, the least altered carbonaceous chondrites are almost devoid of phyllosilicates and rather contain abundant amorphous silicates (Brearley, 1993; Greshake, 1997; Chizmadia and Brearley, 2008; Abreu and Brearley, 2011; Le Guillou and Brearley, 2014; Le Guillou et al., 2014, 2015; Dobrică et al., 2019; Dobrică and Brearley, 2020; Vollmer et al., 2020). Still, these amorphous silicates are intimately associated with diffuse OM, which is generally interpreted as having been transported by fluids during hydrothermal alteration episodes (Le Guillou et al., 2014; Vinogradoff et al., 2017; Changela et al., 2018). By analogy with the present results, it may be suggested that the crystallization of amorphous silicates during hydrothermal alteration was limited by the presence of organic compounds, while amorphous silicates occurring in organic-poor regions would have crystallized faster/easier, producing relatively big particles relatively poor in OM. In addition, the present study suggests that determining the permanent charge of crystalline phyllosilicates associated to elevated contents of diffuse OM may bring additional constraints on their origin and history. In fact, according to the present results, the alteration of pre-existing crystalline phyllosilicates in the presence of organic compounds should produce smectites exhibiting a highly variable permanent charge while the crystallization of initially amorphous materials should produce phyllosilicates exhibiting a less variable permanent charge.

Last, it has been suggested that the SOM fraction recovered by solvent extraction does not represent the entire SOM pool of carbonaceous chondrites (Pearson et al., 2006; Alexander et al., 2017;

Vinogradoff et al., 2020a). Here, 50 wt. % of the initial amount of carbon has not been extracted from the residues using classical solvent extraction. Hence, a significant portion of the chondritic SOM could have been retained in chondritic clays and disregarded, especially since the abundance of smectites in carbonaceous chondrites increases with increasing alteration. The present study thus reinforces the need for *in situ* investigations of OM and/or for the development of new extraction protocols to better document these -so far- unknown chondritic soluble organic compounds.

Acknowledgements

This work was made possible thanks to financial support from the Agence Nationale de la Recherche (RAHIIA_SSOM, ANR-16-CE29-0015) ANR (project RAHIIA_SSOM – Local PI: LR) and by the European Research Council for funding via the ERC project HYDROMA (consolidator grant agreement No. 819587, HYDROMA). This work was supported by the Paris Île-de-France Region.. We thank Elisabeth Malassis for administrative support, Denis Fiorillo for his expert support with EA-IRMS, Imène Esteve for her expert support with the SEM. The authors wish to acknowledge the workforce of the spectroscopic and X-ray diffraction facilities at IMPMC. Special thanks go to Stefan Stanescu and Sufal Swaraj for their expert support with the HERMES STXM beamline at SOLEIL. The SEM facility at IMPMC is supported by Region Ile de France grant SESAME Number I-07-593/R, INSU-CNRS, INP-CNRS and UPMC-Paris 6, and by the Agence Nationale de la Recherche (ANR) grant number ANR-07-BLAN-0124-01. The TEM facility at the CCM (Lille University) is supported by the Chevreul Institute, the European FEDER and Région Nord-Pas-de-Calais. The HERMES beamline (SOLEIL) is supported by the CNRS, the CEA, the Region Ile de France, the Departmental Council of Essonne and the Region Centre. Finally, this manuscript has benefited from constructive comments by Dionysis Foustoukos and one anonymous reviewer , as well as from associate editor Eric Quirico

References

Abreu N. M. and Brearley A. J. (2011) Deciphering the nebular and asteroidal record of silicates and organic material in the matrix of the reduced CV3 chondrite Vigarano: Matrix in the CV3 chondrite Vigarano. *Meteorit. Planet. Sci.* **46**, 252–274.

Aléon J. (2010) Multiple origins of nitrogen isotopic anomalies in meteorites and comets. *Astrophys. J.* **722**, 1342–1351.

Alexander C. M. O., Cody G. D., De Gregorio B. T., Nittler L. R. and Stroud R. M. (2017) The nature, origin and modification of insoluble organic matter in chondrites, the major source of Earth's C and N. *Geochemistry* **77**, 227–256.

Alexander C. M. O., Fogel M., Yabuta H. and Cody G. D. (2007) The origin and evolution of chondrites recorded in the elemental and isotopic compositions of their macromolecular organic matter. *Geochim. Cosmochim. Acta* **71**, 4380–4403.

Alleon J., Bernard S., Le Guillou C., Daval D., Skouri-Panet F., Kuga M. and Robert F. (2017) Organic molecular heterogeneities can withstand diagenesis. *Sci. Rep.* **7**.

Baron F., Petit S. and Decarreau A. (2019) Experimental evidence of the metastability of ferric smectite. *Geochim. Cosmochim. Acta* **265**, 69–84.

Baron F., Petit S., Tertre E. and Decarreau A. (2016) Influence of Aqueous Si and Fe Speciation on Tetrahedral Fe(III) Substitutions in Nontronites: a Clay Synthesis Approach. *Clays Clay Miner.* **64**, 230–244.

Belkhou R., Stanescu S., Swaraj S., Besson A., Ledoux M., Hajlaoui M. and Dalle D. (2015) HERMES: a soft X-ray beamline dedicated to X-ray microscopy. *J. Synchrotron Radiat.* **22**, 968–979.

Bernard S., Benzerara K., Beyssac O., Balan E. and Brown Jr. G. E. (2015) Evolution of the macromolecular structure of sporopollenin during thermal degradation. *Heliyon* **1**, e00034.

Bernstein M. P., Sandford S. A., Allamandola L. J., Chang S. and Scharberg M. A. (1995) Organic Compounds Produced by Photolysis of Realistic Interstellar and Cometary Ice Analogs Containing Methanol. *Astrophys. J.* **454**, 327.

Blazzevjic N., Kolbah D., Belin B., Sunjic V. and Kajfez F. (1979) Hexamethylenetetramine, A Versatile Reagent in Organic Synthesis. *Synthesis* **1979**, 161–176.

Brearley A. J. (2006) The action of water. In Meteorites and the Early Solar System II (eds. D. S. Lauretta and H. Y. McSween). University of Arizona Press, Tucson, pp. 587–624.

Brearley A. J. (1993) Matrix and fine-grained rims in the unequilibrated CO3 chondrite, ALHA77307: Origins and evidence for diverse, primitive nebular dust components. *Geochim. Cosmochim. Acta* **57**, 1521–1550.

Changela H. G., Le Guillou C., Bernard S. and Brearley A. J. (2018) Hydrothermal evolution of the morphology, molecular composition, and distribution of organic matter in CR (Renazzo-type) chondrites. *Meteorit. Planet. Sci.* ***53,*** 1006-1029..

Chizmadia L. J. and Brearley A. J. (2008) Mineralogy, aqueous alteration, and primitive textural characteristics of fine-grained rims in the Y-791198 CM2 carbonaceous chondrite: TEM observations and comparison to ALHA81002. *Geochim. Cosmochim. Acta* **72**, 602–625.

Cliff G. and Lorimer G. W. (1975) The quantitative analysis of thin specimens. *J. Microsc.* **103**, 203–207.

Cody G. D. and Alexander C. M. O. 'D. (2005) NMR studies of chemical structural variation of insoluble organic matter from different carbonaceous chondrite groups. *Geochim. Cosmochim. Acta* **69**, 1085–1097.

Cody G. D., Heying E., Alexander C. M. O., Nittler L. R., Kilcoyne A. L. D., Sandford S. A. and Stroud R. M. (2011) Establishing a molecular relationship between chondritic and cometary organic solids. *Proc. Natl. Acad. Sci. U. S. A.* **108**, 19171–19176.

Cottin H., Szopa C. and Moore M. H. (2001) Production of Hexamethylenetetramine in Photolyzed and Irradiated Interstellar Cometary Ice Analogs. *Astrophys. J.* **561**, L139–L142.

Danger G., Vinogradoff V., Matzka M., Viennet J.-C., Remusat L., Bernard S., Ruf A., Le Sergeant d'Hendecourt L. and Schmitt-Kopplin P. (2021) Exploring the link between molecular cloud ices and chondritic organic matter in laboratory. *Nat. Commun.* **12**, 3538.

Derenne S. and Robert F. (2010) Model of molecular structure of the insoluble organic matter isolated from Murchison meteorite: Model of molecular structure of Murchison IOM. *Meteorit. Planet. Sci.* **45**, 1461–1475.

Dionnet Z., Aleon-Toppani A., Baklouti D., Borondics F., Brisset F., Djouadi Z., Sandt C. and Brunetto R. (2018) Organic and mineralogic heterogeneity of the Paris meteorite followed by FTIR hyperspectral imaging. *Meteorit. Planet. Sci.* **53**, 2608–2623.

Dionnet Z., Brunetto R., Aléon-Toppani A., Rubino S., Baklouti D., Borondics F., Buellet A.-C., Djouadi Z., King A., Nakamura T., Rotundi A., Sandt C., Troadec D. and Tsuchiyama A. (2020) Combining IR and X-ray microtomography data sets: Application to Itokawa particles and to Paris meteorite. *Meteorit. Planet. Sci.* **55,** 1645-1664.

Dobrică E. and Brearley A. J. (2020) Amorphous silicates in the matrix of Semarkona: The first evidence for the localized preservation of pristine matrix materials in the most unequilibrated ordinary chondrites. *Meteorit. Planet. Sci.* **55**, 649–668.

Dobrică E., Le Guillou C. and Brearley A. J. (2019) Aqueous alteration of porous microchondrules in Semarkona: Implications for hydration, oxidation and elemental exchange processes. *Geochim. Cosmochim. Acta* **244**, 292–307.

Dzene L., Verron H., Delville A., Michot L. J., Robert J.-L., Tertre E., Hubert F. and Ferrage E. (2017) Influence of Tetrahedral Layer Charge on the Fixation of Cesium in Synthetic Smectite. *J. Phys. Chem. C* **121**, 23422–23435.

Farmer V. C. ed. (1974) The Infrared Spectra of Minerals. *Mineralogical Society of Great Britain and Ireland*.

Farmer V. C. and Russell J. D. (1971) Interlayer complexes in layer silicates. The structure of water in lamellar ionic solutions. *Trans. Faraday Soc.* **67**, 2737.

Foustoukos D. I. and Stern J. C. (2012) Oxidation pathways for formic acid under low temperature hydrothermal conditions: Implications for the chemical and isotopic evolution of organics on Mars. *Geochim. Cosmochim. Acta* **76**, 14–28.

Garvie L. A. J. and Buseck P. R. (2007) Prebiotic carbon in clays from Orgueil and Ivuna (CI), and Tagish Lake (C2 ungrouped) meteorites. *Meteorit. Planet. Sci.* **42**, 2111–2117.

Gautier M., Muller F. and Le Forestier L. (2017) Interactions of ammonium-smectite with volatile organic compounds from leachates. *Clay Miner.* **52**, 143–158.

Greshake A. (1997) The primitive matrix components of the unique carbonaceous chondrite Acfer 094: A TEM study. *Geochim. Cosmochim. Acta* **61**, 437–452.

Jackson M. L. (1962) Interlayering of Expansible Layer Silicates in Soils by Chemical Weathering. *Clays Clay Miner.* **11**, 29–46.

Jacquemot P., Viennet J.-C., Bernard S., Le Guillou C., Rigaud B., Delbes L., Georgelin T. and Jaber M. (2019) The degradation of organic compounds impacts the crystallization of clay minerals and vice versa. *Sci. Rep.* **9**, 20251.

Kebukawa Y., Chan Q. H. S., Tachibana S., Kobayashi K. and Zolensky M. E. (2017) One-pot synthesis of amino acid precursors with insoluble organic matter in planetesimals with aqueous activity. *Sci. Adv.* **3**, e1602093.

Kebukawa Y. and Cody G. D. (2015) A kinetic study of the formation of organic solids from formaldehyde: Implications for the origin of extraterrestrial organic solids in primitive Solar System objects. *Icarus* **248**, 412–423.

Kebukawa Y., David Kilcoyne A. L. and Cody G. D. (2013) Exploring the Potential Formation of Organic Solids in Chondrites and Comets through Polymerization of Interstellar Formaldehyde. *Astrophys. J.* **771**, 19.

Kebukawa Y., Kobayashi H., Urayama N., Baden N., Kondo M., Zolensky M. E. and Kobayashi K. (2019) Nanoscale infrared imaging analysis of carbonaceous chondrites to understand organic-mineral interactions during aqueous alteration. *Proc. Natl. Acad. Sci. U. S. A.* **116**, 753–758.

Kebukawa Y., Nakashima S., Mita H., Muramatsu Y. and Kobayashi K. (2020) Molecular evolution during hydrothermal reactions from formaldehyde and ammonia simulating aqueous alteration in meteorite parent bodies. *Icarus* **347**, 113827.

Kerridge J. F. (1993) Origins of organic matter in meteorites. *Proceedings of the NIPR Symposium on Antarctic meteorites* **6**, pp. 293-303.

King A. J., Schofield P. F., Howard K. T. and Russell S. S. (2015) Modal mineralogy of CI and CI-like chondrites by X-ray diffraction. *Geochim. Cosmochim. Acta* **165**, 148–160.

Kort M. J. (1970) Reactions of Free Sugars with Aqueous Ammonia. In *Advances in Carbohydrate Chemistry and Biochemistry* Elsevier. pp. 311–349.

Lagaly G., Ogawa M. and Dékány I. (2013) Chapter 10.3 - Clay Mineral–Organic Interactions. In *Developments in Clay Science* (eds. F. Bergaya and Gerhard Lagaly). Handbook of Clay Science. Elsevier. pp. 435–505.

Laird D. A. (1994) Evaluation of the Structural Formula and Alkylammonium Methods of Determining Layer Charge. In *Layer Charge Characteristics of 2:1 Silicate Clay Minerals*, Clay Minerals Society.

Le Guillou C., Bernard S., Brearley A. J. and Remusat L. (2014) Evolution of organic matter in Orgueil, Murchison and Renazzo during parent body aqueous alteration: In situ investigations. *Geochim. Cosmochim. Acta* **131**, 368–392.

Le Guillou C., Bernard S., De la Pena F. and Le Brech Y. (2018) XANES-Based Quantification of Carbon Functional Group Concentrations. *Anal. Chem.* **90**, 8379–8386.

Le Guillou C. and Brearley A. (2014) Relationships between organics, water and early stages of aqueous alteration in the pristine CR3.0 chondrite MET 00426. *Geochim. Cosmochim. Acta* **131**, 344–367.

Le Guillou C., Changela H. G. and Brearley A. J. (2015) Widespread oxidized and hydrated amorphous silicates in CR chondrites matrices: Implications for alteration conditions and H2 degassing of asteroids. *Earth Planet. Sci. Lett.* **420**, 162–173.

Lewan M. D. (1997) Experiments on the role of water in petroleum formation. *Geochim. Cosmochim. Acta* **61**, 3691–3723.

Lewan M. D. and Roy S. (2011) Role of water in hydrocarbon generation from Type-I kerogen in Mahogany oil shale of the Green River Formation. *Org. Geochem.* **42**, 31–41.

McCollom T. M. (2013) The influence of minerals on decomposition of the n-alkyl-α-amino acid norvaline under hydrothermal conditions. *Geochim. Cosmochim. Acta* **104**, 330–357.

McCollom T. M., Lollar B. S., Lacrampe-Couloume G. and Seewald J. S. (2010) The influence of carbon source on abiotic organic synthesis and carbon isotope fractionation under hydrothermal conditions. *Geochim. Cosmochim. Acta* **74**, 2717–2740.

Mccollom T. and Seewald J. (2006) Carbon isotope composition of organic compounds produced by abiotic synthesis under hydrothermal conditions. *Earth Planet. Sci. Lett.* **243**, 74–84.

McSween H. Y. (1979) Alteration in CM carbonaceous chondrites inferred from modal and chemical variations in matrix. *Geochim. Cosmochim. Acta* **43**, 1761–1770.

Meissner F., Schwiedessen E. and Othmer D. F. (1954) Continuous Production of Hexamethylenetetramine. *Ind. Eng. Chem.* **46**, 724–727.

Morris P. L. (1980) The correction of thin foil microanalysis data for X-ray absorption effects. *Electron Microscopy and Analysis 1979*, 413–416.

Nagendrappa G. (2011) Organic synthesis using clay and clay-supported catalysts. *Appl. Clay Sci.* **53**, 106–138.

Nagendrappa G. and Chowreddy R. R. (2021) Organic Reactions Using Clay and Clay-Supported Catalysts: A Survey of Recent Literature. *Catal. Surv. Asia* **25**, 231–278.

679 Nittler L. R., Stroud R. M., Trigo-Rodríguez J. M., De Gregorio B. T., Alexander C. M. O., Davidson J.,
680 Moyano-Cambero C. E. and Tanbakouei S. (2019) A cometary building block in a primitive
681 asteroidal meteorite. *Nat. Astron.* **3**, 659–666.
682 Pan C., Geng A., Zhong N., Liu J. and Yu L. (2009) Kerogen pyrolysis in the presence and absence of water
683 and minerals: Amounts and compositions of bitumen and liquid hydrocarbons. *Fuel* **88**, 909–919.
684 Pearson V. K., Sephton M. A., Franchi I. A., Gibson J. M. and Gilmour I. (2006) Carbon and nitrogen in
685 carbonaceous chondrites: Elemental abundances and stable isotopic compositions. *Meteorit. Planet.*
686 *Sci.* **41**, 1899–1918.
687 de la Pena F., Ostasevicius T., Tonaas Fauske V., Burdet P., Jokubauskas P., Nord M., Sarahan M., Prestat
688 E., Johnstone D. N., Taillon J., Jan Caron, Furnival T., MacArthur K. E., Eljarrat A., Mazzucco S.,
689 Migunov V., Aarholt T., Walls M., Winkler F., Donval G., Martineau B., Garmannslund A.,
690 Zagonel L.-F. and Iyengar I. (2017) Electron Microscopy (Big and Small) Data Analysis With the
691 Open Source Software Package HyperSpy. *Microsc. Microanal.* **23**, 214–215.
692 Petit S., Baron F. and Decarreau A. (2017) Synthesis of nontronite and other Fe-rich smectites: a critical
693 review. *Clay Miner.* **52**, 469–483.
694 Pizzarello S., Cooper G. W. and Flynn G. J. (2006) The nature and distribution of the organic material in
695 carbonaceous chondrites and interplanetary dust particles. *Meteorites and the early solar system II*
696 **1**, 625–651.
697 Remusat L. (2015) Organics in primitive meteorites. *EMU notes in Mineralogy* **15**, 33–65.
698 Remusat L., Bonnet J.-Y., Bernard S., Buch A. and Quirico E. (2019) Molecular and isotopic behavior of
699 insoluble organic matter of the Orgueil meteorite upon heating. *Geochim. Cosmochim. Acta* **263**,
700 235–247.
701 Remusat L., Derenne S. and Robert F. (2005a) New insight on aliphatic linkages in the macromolecular
702 organic fraction of Orgueil and Murchison meteorites through ruthenium tetroxide oxidation.
703 *Geochim. Cosmochim. Acta* **69**, 4377–4386.
704 Remusat L., Derenne S., Robert F. and Knicker H. (2005b) New pyrolytic and spectroscopic data on Orgueil
705 and Murchison insoluble organic matter: A different origin than soluble? *Geochim. Cosmochim.*
706 *Acta* **69**, 3919–3932.
707 Remusat L., Guan Y., Wang Y. and Eiler J. M. (2010) Accretion and preservation of D-rich organic particles
708 in carbonaceous chondrites: evidence for important transport in the early Solar System nebula.
709 *Astrophys. J.* **713**, 1048–1058.
710 Remusat L., Robert F., Meibom A., Mostefaoui S., Delpoux O., Binet L., Gourier D. and Derenne S. (2009)
711 Proto-planetary disk chemistry recorded by D-rich organic radicals in carbonaceous chondrites.
712 *Astrophys. J.* **698**, 2087–2092.
713 Ricardo A. (2004) Borate Minerals Stabilize Ribose. *Science* **303**, 196–196.
714 Robert F. and Epstein S. (1982) The concentration and isotopic composition of hydrogen, carbon and
715 nitrogen in carbonaceous meteorites. *Geochim. Cosmochim. Acta* **46**, 81–95.
716 Robert M., Razzaghe M., Vicente M. A. and Veneau G. (1979) Role du facteur biochimique dans l'alteration
717 des mineraux silicates. *Bulletin de l'Association Française pour l'Etude du Sol*, 153–174.
718 Schwertmann U. (1966) Inhibitory Effect of Soil Organic Matter on the Crystallization of Amorphous Ferric
719 Hydroxide. *Nature* **212**, 645–646.
720 Seewald J. S. (2001) Aqueous geochemistry of low molecular weight hydrocarbons at elevated temperatures
721 and pressures: constraints from mineral buffered laboratory experiments. *Geochim. Cosmochim.*
722 *Acta* **65**, 1641–1664.
723 Sephton M. A. (2014) Organic Geochemistry of Meteorites. In *Treatise on Geochemistry (Second Edition)*
724 (eds. H. D. Holland and K. K. Turekian). Elsevier, Oxford. pp. 1–31.
725 Swaraj S., Belkhou R., Stanescu S., Rioult M., Besson A. and Hitchcock A. P. (2017) Performance of the
726 HERMES beamline at the carbon K-edge. *Journal of Physics: Conference Series* **849**, 012046.
727 Viennet J.-C., Bernard S., Le Guillou C., Jacquemot P., Balan E., Delbes L., Rigaud B., Georgelin T. and
728 Jaber M. (2019) Experimental clues for detecting biosignatures on Mars. *Geochem. Persp. Let.*, 28–
729 33.

730 Viennet J.-C., Bernard S., Le Guillou C., Jacquemot P., Delbes L., Balan E. and Jaber M. (2020) Influence
731 of the nature of the gas phase on the degradation of RNA during fossilization processes. *Appl. Clay*
732 *Sci.* **191**, 105616.
733 Viennet J.-C., Hubert F., Ferrage E., Tertre E., Legout A. and Turpault M.-P. (2015) Investigation of clay
734 mineralogy in a temperate acidic soil of a forest using X-ray diffraction profile modeling: Beyond
735 the HIS and HIV description. *Geoderma* **241–242**, 75–86.
736 Viennet J.-C., Hubert F., Tertre E., Ferrage E., Robin V., Dzene L., Cochet C. and Turpault M.-P. (2016)
737 Effect of particle size on the experimental dissolution and auto-aluminization processes of K-
738 vermiculite. *Geochim. Cosmochim. Acta* **180**, 164–176.
739 Vinogradoff V., Bernard S., Le Guillou C. and Remusat L. (2018) Evolution of interstellar organic
740 compounds under asteroidal hydrothermal conditions. *Icarus* **305**, 358–370.
741 Vinogradoff V., Duvernay F., Danger G., Theulé P. and Chiavassa T. (2011) New insight into the formation
742 of hexamethylenetetramine (HMT) in interstellar and cometary ice analogs. *Astronomy &*
743 *Astrophysics* **530**, A128.
744 Vinogradoff V., Le Guillou C., Bernard S., Binet L., Cartigny P., Brearley A. J. and Remusat L. (2017)
745 Paris vs. Murchison: Impact of hydrothermal alteration on organic matter in CM chondrites.
746 *Geochim. Cosmochim. Acta* **212**, 234–252.
747 Vinogradoff V., Le Guillou C., Bernard S., Viennet J.-C., Jaber M. and Remusat L. (2020a) Influence of
748 phyllosilicates on the hydrothermal alteration of organic matter in asteroids: Experimental
749 perspectives. *Geochim. Cosmochim. Acta* **269**, 150–166.
750 Vinogradoff V., Remusat L., McLain H. L., Aponte J. C., Bernard S., Danger G., Dworkin J. P., Elsila J. E.
751 and Jaber M. (2020b) Impact of Phyllosilicates on Amino Acid Formation under Asteroidal
752 Conditions. *ACS Earth Space Chem.* **4**, 1398–1407.
753 Vollmer C., Kepaptsoglou D., Leitner J., Busemann H., Spring N. H., Ramasse Q. M., Hoppe P. and Nittler
754 L. R. (2014) Fluid-induced organic synthesis in the solar nebula recorded in extraterrestrial dust
755 from meteorites. *Proc. Natl. Acad. Sci. U. S. A.* **111**, 15338–15343.
756 Vollmer C., Leitner J., Kepaptsoglou D., Ramasse Q. M., Busemann H. and Hoppe P. (2020) Isotopic
757 compositions, nitrogen functional chemistry, and low-loss electron spectroscopy of complex
758 organic aggregates at the nanometer scale in the carbonaceous chondrite Renazzo. *Meteorit. Planet.*
759 *Sci.* **55**, 1293–1319.
760 Wang J., Morin C., Li L., Hitchcock A. P., Scholl A. and Doran A. (2009) Radiation damage in soft X-ray
761 microscopy. *J. Electron Spectrosc. Relat. Phenom.* **170**, 25–36.
762 Weber A. L. (2001) The Sugar Model: Catalysis by Amines and Amino Acid Products. *Orig. Life Evol.*
763 *Biosph.* **31**, 71–86.
764 Wilson M. J. (1999) The origin and formation of clay minerals in soils: past, present and future perspectives.
765 *Clay miner.* **34**, 7–25.
766 Yabuta H., Williams L. B., Cody G. D., Alexander C. M. O. and Pizzarello S. (2007) The insoluble
767 carbonaceous material of CM chondrites: A possible source of discrete organic compounds under
768 hydrothermal conditions. *Meteorit. Planet. Sci.* **42**, 37–48.
769 Yariv S. and Cross H. (2001) *Organo-clay complexes and interactions*. CRC Press.
770 Yesiltas M. and Kebukawa Y. (2016) Associations of organic matter with minerals in Tagish Lake meteorite
771 via high spatial resolution synchrotron-based FTIR microspectroscopy. *Meteorit. Planet. Sci.* **51**,
772 584–595.
773